JOURNAL OF CATALYSIS 42, 139–147 (1976)

Chemical Reactivity of Supported Gold

III. Atomic Binding and Coordination of Gold from X-Ray Absorption Fine Structure Spectroscopy[1]

I. W. BASSI

Istituto Donegani, Novara, Italy

F. W. LYTLE

Boeing Aerospace Company, Seattle, Washington

AND

G. PARRAVANO[2]

Department of Chemical Engineering, University of Michigan, Ann Arbor, Michigan 48104

Received September 26, 1975

Preparations of Au and Pt supported on Al_2O_3, MgO, and SiO_2 were subjected to analysis by extended X-ray absorption fine structure spectroscopy (EXAFS). The samples contained 0.20, 5.00, and 8.00 wt% Au, and 5.00 wt% Pt. Metal dispersion ranged between 0.3 to 45%. Anisotropic growth was detected in the larger particles. The L_{III} X-ray absorption coefficient was normalized to the same atom basis and Fourier transformed to yield the radial structure function for each preparation. From bond distance comparison with reference materials, assignments were made to specific peaks of the radial structure function.

The analysis of the results showed that the metals were present in two distinct phases: metallic with coordination and metal-to-metal distance characteristic of bulk Au, and Pt (particulate phase), and a highly disperse one (dissolved phase). It was concluded that the latter consisted of metal atomically dispersed, or condensed in small, flat clusters of a few atoms. It was further estimated that the majority of Au and Pt was present in the highly disperse form, i.e., 60% for Au and 86% for Pt. Au atoms did not simply substitute Mg in the MgO matrix to form the dissolved Au–MgO phase and they carried an average charge +1.

In previous researches on supported Au microparticles it was found that the onset of chemical reactivity in Au metal was dependent upon the nature of the support, the size of the microparticles and their preparation method (*1*). In hydrogen (*2*) and oxygen (*1*) transfer reactions, the activity of supported Au was found to be comparable to that of Pt. Supported Au has already achieved a position of commercial importance in the process industry as a catalytic partner in industrial chemical processes (*3*). Despite the interesting catalytic performance and increasing industrial applications, it has not yet been possible to clarify the physical and chemical phenomena associated with the size and the morphology of supported Au particles whose reactivity stands in drastic contrast to the inertness of the massive metal.

[1] Previous articles in this series: *J. Catal.* **18**, 200, 320 (1970).

[2] To whom all queries about this paper should be addressed.

From a preliminary review of the structural and morphological problem of supported Au it was concluded that three microparticle parameters needed a thorough inspection for their possible key role in controlling the state of the metal and therefore its reactivity in the supported preparations, namely: the Au–Au distance, the coordination around an Au atom (number and nature of nearest neighbors), and the electron binding energy of Au. In this direction, it appeared to us that X-ray absorption fine structure spectroscopy (EXAFS) could successfully contribute to the derivation of a realistic model for the Au system that could include the role of the above parameters. EXAFS is eminently suited to explore the surroundings of the absorbing Au atom and to provide the radial structure function centered on the atom of interest. This function gives direct information on the nature and number of coordinating atoms (*4*). Under favorable circumstances, from EXAFS it is also possible to derive energy shifts in the absorption edge relative to the bulk metal that are indicative of the nature of the binding of the atoms. Although the determination of the electron binding energy through EXAFS is not direct and detailed as through ESCA, the possibility of the simultaneous measurement of the radial structure function and of the electron binding energy on the same sample and under exactly similar experimental conditions provides an important simplification and a powerful tool to increase the consistency of the measurements.

EXPERIMENTAL METHODS

Materials. Three samples of supported Au were investigated: A 1141, Au on η-Al_2O_3 (Davison, surface area 230 m^2/g), prepared by Al_2O_3 impregnation with aqueous solution of $HAuCl_4 \cdot 3H_2O$ (Baker Co.), followed by reduction with 2% oxalic acid solution at 40°C, filtered, washed, dried, and heated at 350°C, 2 hr, 0.1 Torr; A 1211, and A 1241 Au on MgO (reagent grade, surface area 18 m^2/g), preparation similar to that employed for A 1141.

Materials employed as references for Au were: Au foil (2.5 thick, rolled from 99.9% Au); $HAuCl_4 \cdot 3H_2O$ (Baker); Au_2O_3 (Research Organic/Inorganic Chemical Corp.). Since Pt and Au are adjacent elements in the periodic table similar EXAFS properties should be expected (absorption edge, phase shift, magnitude normalization, etc.). Pt provides also an interesting comparison to a related supported catalyst system. It was then decided to include supported Pt as a reference material. Pt preparations employed were as follows: 5% Pt on Cab-O-Sil, prepared by impregnation from a H_2PtCl_6 solution followed by reduction by H_2 at 500°C. $PtCl_2$ (Matthey Bishop); α-PtO_2 prepared according to a literature method (*5*) and Pt foil (2.5 thick, 99.9% Pt).

Equipment. X-Ray absorption experiments were carried out with an X-ray tube with an Ag target, a LiF monochromator and a Xe filled proportional counter.

Procedure. Samples were mounted within a dry box into a cell with Mylar windows, the cell was pumped down to the 10^{-6} Torr and cooled to 77°K for the duration of the X-ray measurements. Approximately 10 passes through each absorption edge (20 passes for A 1211) were averaged to obtain the desired statistics. The L_{III} absorption edge was measured for both metals. The phase shift, which appears in the expression of the radial structure function and it is related to electron vacancies in the absorbing atom, was derived from standard materials following a procedure already described (*4*). For the first coordination shell of the standard material one has (*4*)

$$\frac{\mathrm{Mag}_s \cdot r_{1s}^2}{N_{1s}} = C = \text{constant},$$

where Mag_s is the magnitude of the first

peak of the Fourier transform of the EXAFS data of the standard material, r_{1s} its distance (Å) (after correction to take into account the phase shift) from the absorbing atom ($r = 0$), and N_{1s} is the coordination number relative to the first shell. Once C is defined for the standard material, the coordination number, N_1, for the first shell of the unknown material is given by:

$$N_{1x} = \frac{\mathrm{Mag}_x \cdot r_{1x}^2}{C},$$

where Mag_x and r_{1x} have the same meaning as before but are now the values defined for the unknown material. Data were normalized to separate EXAFS information from the background and reduced thus to a per atom basis (*4*). The normalized EXAFS data for the reference materials and the supported Au samples were Fourier transformed to obtain structure functions containing information on interatomic distances and coordination numbers (*4*).

Supported Gold and Reference Materials Characterization

X-Ray diffraction patterns of supported Au preparations showed peaks of both metallic Au and support material. Particle size of supported Au and Pt obtained from X-ray line broadening is reported in Table 1 together with sample composition (by atomic absorption).

Since A 1141 presented very sharp X-ray diffraction lines, measurements on the side of the unit cell were performed on this sample. The value found was 4.0799 Å, while that for bulk metallic gold is 4.0786 Å (*6*). This indicates that Au particles had a well defined metallic structure. Au particle size was measured for this sample on the (200), (400), (111), and (222) lines. It was found that in the direction ⊥ to the (111) plane particle size was 2200 Å, while in the direction ⊥ to the (200) plane was 1300 Å. This is an indication that particle growth did not occur isotropically—faster growth took place in the direction ⊥ to the octahedral (111) plane. It is likely that the anisotropy in particle growth, which is somewhat surprising for particles of this size, has also contributed to a nonstatistical distribution of crystal planes at the surface.

TABLE 1

Particle Diameter,[a] D, Dispersion of Supported Au and Pt Preparations

Sample	Metal (wt%)	D (Å)	Dispersion (%)
A 1241	5.00	100	9
A 1141	8.00	1300–2200	0.6
A 1211	0.20	20	45
Pt	5.00	50	18

[a] Calculated assuming spherical shape.

The metallic Au foil and $HAuCl_4 \cdot 3H_2O$ were of known crystal structure; however, Au_2O_3 was of dubious crystallinity. Its X-ray diffraction showed only a trace of broad Au peaks. The problem of crystallization of Au_2O_3 has been discussed previously (*7*) and the Au–O distance of 2.04 Å found by these authors was assumed for the present Au_2O_3 sample.

RESULTS

The oscillatory part of the L_{III} X-ray absorption coefficient $\chi(K)$ normalized

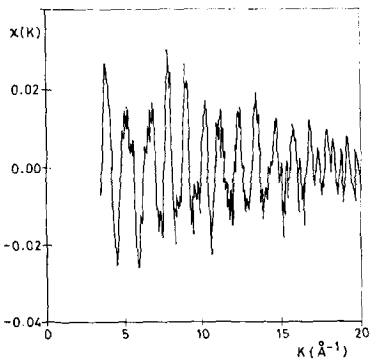

FIG. 1. X-Ray absorption coefficient $\chi(K)$, of metallic Au plotted vs the photoelectron wave vector, K.

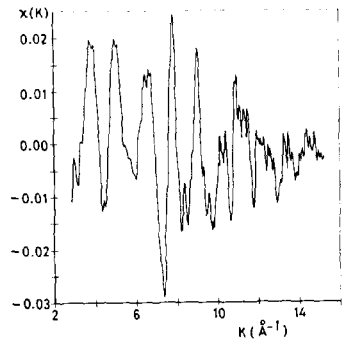

FIG. 2. X-Ray absorption coefficient $\chi(K)$, of Au in A 1141 plotted vs photoelectron wavevector, K.

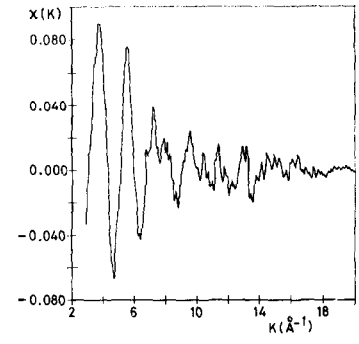

FIG. 4. X-Ray absorption coefficient, $\chi(K)$, of Pt in Pt-SiO_2 plotted vs photoelectron wavevector, K.

to the same atom basis of metallic Au, plotted versus the photoelectron wave vector K is reported in Fig. 1. In Figs. 2, 3, and 4, similar plots for A 1141, A 1121, and Pt on Cab-O-Sil are presented. The magnitude of the K^3 Fourier transform of $\chi(K)$ plotted versus the radial distance from the absorbing atom, r for metallic Au is shown in Fig. 5. This is the EXAFS spectrum of Au. The numbers over the peaks locate the first seven coordination shells of metallic Au. The constant phase shift is clearly noticeable. In Figs. 6 to 12 we report similar plots for $HAuCl_4 \cdot 3H_2O$, Au_2O_3, A 1241, A 1141, A 1211, metallic Pt and Pt on Cab-O-Sil. Results of the computations for the distances between Au atoms and those in the first coordination sphere, r_1, and their coordination number, N, are collected in Table 2. The r_1 distances were corrected for the phase shift observed for the reference materials, i.e., 0.15 Å for Au–Au and 0.38 Å for Au–O and Au–Cl. For Pt–Pt the value is 0.14 Å, while for Pt–O, Pt–Cl 0.33 Å. The fact that more than one distance is found for r_1 in the catalysts indicates that more than one Au phase is present and the environment is generally complex.

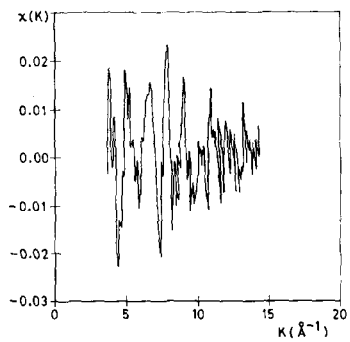

FIG. 3. X-Ray absorption coefficient, $\chi(K)$, of Au in A 1211 plotted vs photoelectron wavevector, K.

DISCUSSION

From EXAFS results three separate distances were qualitatively observed for the first coordination shell of Au in the supported Au preparations (Table 2), a strong Au–Au distance varying from 2.89 to 3.08 Å (this variation is larger than the normal error or 0.06), and two weaker ones:

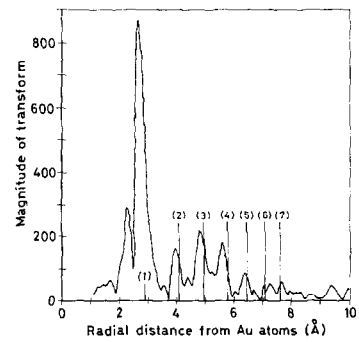

FIG. 5. Magnitude of the K^3 Fourier transform of $\chi(K)$, plotted vs the radial distance from the absorbing atom, r' for metallic Au. The numbers over the peaks locate the first seven coordination shells of metallic Au.

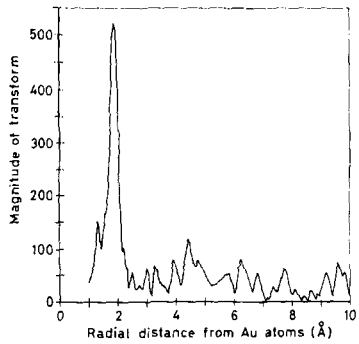

FIG. 6. Magnitude of the K^3 Fourier transform of $\chi(K)$ vs r' for $HAuCl_4 \cdot 3H_2O$.

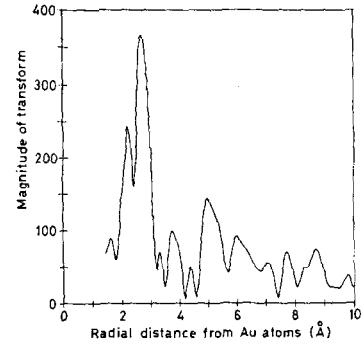

FIG. 8. Magnitude of the K^3 Fourier transform of $\chi(K)$ vs r' for A 1241.

2.00 to 2.35 and 1.61 to 1.77 Å. The first is assigned to the Au–Au bonding, while the second and the third to Au–O or Au–Cl bonding. These assignments were made strictly by bond distance comparison to standard materials. In A 1211 the 3.75 Å distance probably indicates a second neighbor. The difference between samples A 1241 and A 1211 is instructive. Both are supported on MgO, A 1241 has 100 Å Au particles, while A 1211 has 20 Å Au particles. Both show strong metallic Au peaks (Figs. 8 and 10), A 1211 has a longer Au–Au distance, which may be evidence of lattice distortion due to interaction with the support. The very strong peak at 1.61 Å on A 1211 compared to 1.77 Å on A 1241 is taken as evidence of more bonding to the support in this more disperse sample. The two additional peaks at 2.00 and 2.30 Å in A 1241 have been identified with an oxygen distance and the resolution of the electronic $p \rightarrow s$ transition in Au (*4*), respectively. The distance at 2.00 Å in A 1141 was assigned to the Au–O bond, since from the Fourier transform of the Au_2O_3 standard the distance Au^{3+}–O^{2-} was determined to be 2.04 Å. The twin peak appearing to the left of each major peak, which is most apparent in the Au spectrum (Fig. 5) and is due to the $p \rightarrow d$ and $p \rightarrow s$ electronic transitions (*8*), has been accounted for in these peak assignments. In addition to the $p \rightarrow s$ effect, the 2.62 Å peak in the Fourier transform of A 1141 (Table 2) may also be assigned to a Au^+–O^{2-} distance. In fact from the ionic radii (*9*) one has: $r_{Au^+} + r_{O^{2-}} = 1.37 + 1.35 = 2.72$ Å. The Au–Au average coordination of 5 in A 1241 and A 1141 can be used, together with the

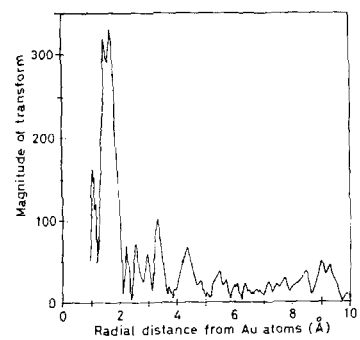

FIG. 7. Magnitude of the K^3 Fourier transform of $\chi(K)$ vs r' for Au_2O_3.

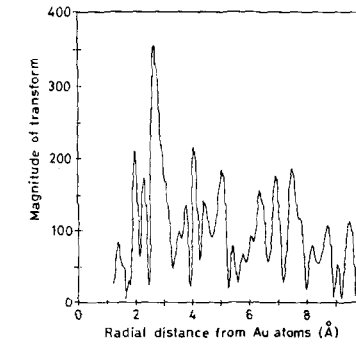

FIG. 9. Magnitude of the K^3 Fourier transform of $\chi(K)$ vs $2'$ for A 1141.

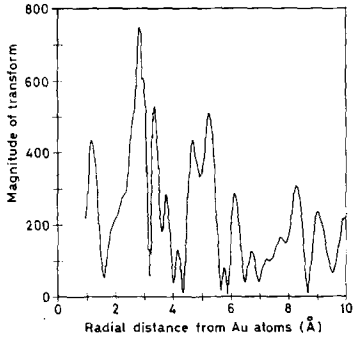

FIG. 10. Magnitude of the K^3 Fourier transform of $\chi(K)$ vs r' for A 1211.

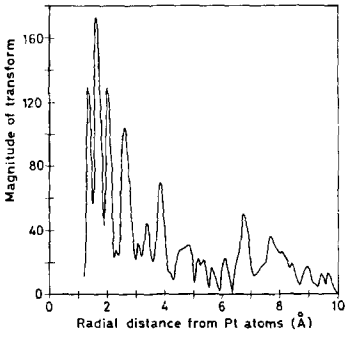

FIG. 12. Magnitude of the K^3 Fourier transform of $\chi(K)$ vs r' for Pt on Cab-O-Sil.

known particle size, to determine the fraction of Au present in the metallic phase. (The coordination number of about 11 for A 1211 seems to be erroneous, probably due to normalization errors due to low metal concentration. Only the characteristic distances were used in interpreting the results for this sample.) Assuming that it is possible to weight additively the surface and bulk coordination numbers, 6 and 12, respectively, according to the corresponding atom fraction, from the X-ray dispersion results reported in Table 1 one may calculate the average Au–Au coordination in each sample. Dividing this average coordination by the number of atoms in the first coordination sphere corresponding to the Au–Au distances calculated for each Au preparation (Table 2), the percentage of the total Au present in the condensed metallic phase is obtained. The results of these calculations are collected in Table 3. The interesting result is that for A 1241 and A 1141 and Pt–SiO_2, only 44, 41, and 14%, respectively, of the metal Au was present in the metallic phase. To confirm this conclusion an independent

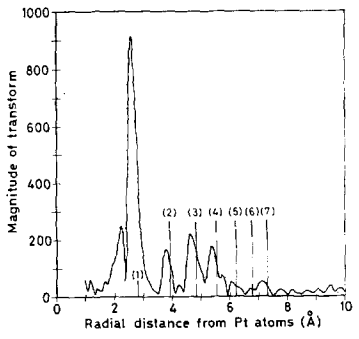

FIG. 11. Magnitude of the K^3 Fourier transform of $\chi(K)$ vs r' for metallic Pt. The numbers over the peaks locate the first seven coordination shells of metallic Pt.

TABLE 2

Distance, r_1, and Number of Atoms, N, in the First Coordination Sphere of Au and Pt in Supported Au and Pt Preparations and Salts

Sample	r_1 (Å)	N	Type of atom
A 1241	1.77	0.4	
	2.35	1.8	O or Cl
	2.89	4.6	Au
A 1141	2.00	0.5	O
	2.62	2.6	
	2.93	4.9	Au
A 1211	1.61	1.7	
	3.08	11.1	Au
	3.75	11.3	Au
Au foil	2.88	12	Au
$HAuCl_4 \cdot 3H_2O$	2.29	4	
Au_2O_3	1.93	2	
	2.12	2	
Pt	2.77	12	
$PtCl_2$	2.32	4	
Pt (5 wt%)	1.72	0.6	
	2.03	1.2	O
	2.38	1.2	Cl
	2.76	1.4	Pt

TABLE 3

Average Au–Au Coordination Number for Supported Au Samples and Percentage of Total Au Present in the Metallic Phase, *M*, for Supported Au and Pt Preparations

Sample	Av coordination No. of Au and Pt	*M* (%)
A 1241	10.4	44
A 1141	12.0	41
A 1211	7.8	—
Cluster (5.8 Å diam)	1.7	—
Pt–SiO_2	9.7	14

measurement of the particulate phase by X-ray diffraction was carried out on a severely sintered A 1141 sample (700°C, 3 hr, 1 atm, air). A quantitative X-ray analysis of the amount of metallic Au was performed by the internal standard method. The relative intensities of the diffraction lines were determined from microphotometric traces of Debye–Scherrer patterns. The internal standard was CaF_2. The results are reported in Table 4. In the last column of Table 4, the ratios between intensities of the sintered and fresh sample are reported. The ratio clearly shows that in the sintered A 1141 sample the content in metallic Au was almost 30–35% by weight higher than in the original A 1141 sample. This is taken to correspond to the amount of dispersed Au which was not in the metallic phase before sintering. This value is in fairly good agreement with the data found by means of the EXAFS analysis.

We conclude that in the two preparations, A 1211, A 1141, and in Pt–SiO_2, Au and Pt were present in two distinct phases: (a) microparticle, structurally similar to metallic Au and Pt and (b) atomically dispersed or in two dimensional clusters. Assuming a cluster of 5.8 Å diameter made out of 7 atoms (a center atom surrounded by 6 atoms in the same plane) it is easily shown that the total coordination number for nonmetallic coordination shown in Table 2 for Au may be fully accounted for.

If we examine closely the nature of the Au dispersed phase in supported A 1241, A 1211 (both MgO supported), it is realized that the short bond distance (1.77 and 1.61 Å) does not represent a simple replacement of Mg by Au in MgO. In fact, the Mg–O bond distance in MgO is 2.11 Å (*9*). An Au atom substitutionally placed at the center of the (100) or of the unit cube of Mg would have neighbors at 1.49 and 1.82 Å, respectively. To identify definitively the positions of Au in the MgO lattice it would be necessary to carry out other quantitative measurements of the effect of temperature on bond distance. In the Al_2O_3 supported sample (A 1141) the situation is more clear. In fact, the peak at 2.00 Å is appropriate for atoms in an octahedral hole. Information on Au location is important, since Au reactivity in chemisorption and catalysis is expected to depend upon the effect of the matrix crystal field on the Au electronic levels.

The observed values of the L_{III} edge shifts, which are surprisingly small in relation to the *K* series (III), are collected in Table 5.

The large experimental error and the complex coordination of the samples make a quantitative interpretation of the shifts

TABLE 4

Relative X-Ray Diffraction Intensities of Fresh and Sintered A 1141 Samples

Au	Relative Intensity[a] fresh	sintered	Fresh/ sintered
(111)	79	109	0.72
(200)	33	49	0.67
(220)	26	38	0.68
(311)	19	32	0.59

[a] Peak intensities averaged from two X-ray diffraction experiments made on two different specimens of the same sample.

TABLE 5

Chemical Shifts of L_{III} Absorption Edge, E, for Au and Pt Materials

Material	E (eV)
Au	0.0 ± 1.5
$HAuCl_4 \cdot 3H_2O$	−3.0
Au_2O_3	−3.4
A 1241	−0.8
A 1141	−2.0
A 1211	−0.5
Pt	0.0 ± 1.5
$PtCl_2$	+1.5
PtO_2	+0.9
Pt–SiO_2	−0.1

impossible. The interesting and yet unexplained result is their negative values. Among the Au samples, A 1141 is unique in having a much higher shift than A 1241 and A 1211. It is tempting to relate the difference in the chemical shift to binding with the support. To illuminate this point we have computed the charge that appears at the periphery of an absorption atom of valence z as a result of being chemically bonded to n near neighbor atoms by means of a chemical bond of degree of covalence C. This charge, called the effective coordination charge, η, is given by $\eta = z - Cn$ (*10*). A smooth correlation has been reported between η and the L_{III} absorption edge of Nd in several salts (*11*). C was calculated from the expression $C = 1 - i$,

TABLE 6

Chemical Valence, z, Coordination, n, and Effective Coordination Charge η for Au Preparations

Material	Ion	z	$X_A - X_B$ (eV/2.8)	n	η
Au_2O_3	Au^{3+}	3	1.80	4	+1.05
	O^{2-}	2	3.50		
$HAuCl_4 \cdot 3H_2O$	A^{3+}	3	1.80	4	−0.05
	Cl^-	5	2.83		
A 1141	A^{3+}	3	1.42	6	+0.08
	O^{2-}	2	3.50		
	Au^{1+}	1	5.42	6	−1.03
	O^{2-}	2	3.50		

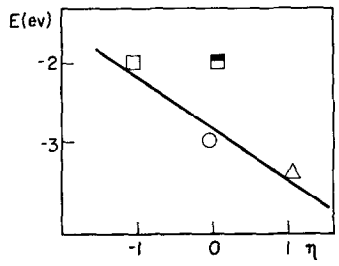

FIG. 13. Effective coordination charge, η, and chemical shift E, for the L_{III} absorption edge in A 1141 and Au compounds, (□) A 1141 (as Au^+), (■) A 1141 (as Au^{3+}), (○) $HAuCl_4 \cdot 3H_2O$, (△) Au_2O_3.

where i is given by (*9*):

$$i = \exp\left[\tfrac{1}{4}(X_A - X_B)^2\right],$$

where X_A, X_B are the electronegativities of the atoms. We have carried out these calculations for Au_2O_3, $HAuCl_4 \cdot 3H_2O$ and A 1141. The results of the calculations are reported in Table 6. Using the values of the L_{III} absorption edge shifts, E, reported in Table 5, the correlation between E and η is presented in Fig. 13. Considering the semiempirical character of the correlation, and the experimental error in the quantitative determination of the edge shift, a fairly linear relationship is obtained. Interestingly, the correlation points to Au^+ as the most likely charge state of Au atomically dispersed in the Al_2O_3 matrix. Support for this conclusion may also be found in the fact that Au^{3+} in alkali metal oxoaurates has been found to have a coordination number of 4 (*12*), inconsistent with the values reported in Table 2.

In previous studies on supported Au catalysts by means of Mössbauer spectroscopy (*13*), it was discovered that isomer shifts more negative than metallic Au and Au^{3+} (in the starting salt) were obtained with supported Au catalysts, when treated under selected conditions of time–temperature–atmosphere. Essentially, tracing the Au isomer shift during preparative conditions, it was found that treatment at 370°C for 3 hr in air produced an isomer

shift more negative than that corresponding to metallic Au. Such a shift resulted from an *s* electron density at the nucleus lower than that of Au metal, and it was suggested that it may have represented Au in strongly electronegative environment. This, of course, is also the conclusion drawn for the present Au preparations via EXAFS analysis. Furthermore, it seems reasonable to suggest that Au^+, obtained by removal of one *s* electron from the $d^{10}s$ electronic configuration of Au, should have a lower *s* electron density than the metal and, consequently, should show Mössbauer isomer shift at more negative velocities. It seems, therefore, that the model of supported Au, which emerges from the present results is consistent with and supported by results obtained by means of Mössbauer spectroscopy.

CONCLUSION

The EXAFS analysis of supported Au samples has confirmed the presence of highly dispersed Au (dissolved phase) and of large metal particles (particulate phase). The former consisted of Au atomically dissolved or present in small, flat clusters. Despite the structurally complex nature of the supported samples fine chemical and structural aspects emerged; the description of the environment of the Au atoms was obtained with a richness of details not achieved before and unmatched by other techniques employed for characterization of supported metal samples.

The results obtained pose several questions on the nature and properties of supported metal catalysts. What are the factors involved in the stabilization of atomically dispersed Au and Pt in Al_2O_3, MgO, and SiO_2? What is the nature of the Au-support electronic interaction, which tends to favor a lower valence state of Au? What is a realistic model for the Au–Al_2O_3, Au–MgO and Pt–SiO_2 "solid solution"? What are the preparative factors which control the ratio between the disperse and the particulate (microparticle) phase? What is the relative chemical reactivity of the two phases? Are all the Au atoms of the dissolved phase in a nonporous support (MgO) available to gas adsorption? This is an important question in calculations of metal dispersion by gas adsorption and reaction rates per unit metal surface area. In the context of the present work, the EXAFS technique will most likely play a leading role in clarifying these and related problems.

ACKNOWLEDGMENT

We thank Mr. M. Calcaterra and Mr. V. Bozzola for the X-ray diffraction measurements and Professor P. Corradini for helpful suggestions.

REFERENCES

1. Cha, D. Y., and Parravano, G., *J. Catal.* **18**, 200 (1970).
2. Parravano, G., *J. Catal.* **18**, 320 (1970).
3. Farbenfabriken Bayer, A. G., *Belgian Pat.* No. 627,888, 1967.
4. Lytle, F. W., Sayers, D. E., and Stern, E. A., *Phys. Rev. B* **11**, 4825, 4836 (1975); Lytle, F. W., Sayers, D. E., and Moore, E. B., *Appl. Phys. Lett.* **24**, 45 (1974).
5. Hoekstra, H. R., and Siegel, S., *Inorg. Chem.* **7**, 141 (1968).
6. Wyckoff, R. W. G., "Crystal Structures," Vol. 1, p. 15. Wiley (Interscience), New York, 1960.
7. Mueller, O., Newnham, R. E., and Ray, R., *J. Inorg. Nucl. Chem.* **31**, 2966 (1969).
8. Lytle, F. W., Sayers, D. E., and Stern, E. A., *Phys. Rev. Lett.*, submitted.
9. Pauling, L., "The Nature of Chemical Bond." Cornell Univ. Press, Ithaca, N. Y., 1948.
10. Batsanov, S. S., "Electronegativity of Elements and Chemical Bonds." Novosibirsk, 1962, USSR Academy of Science Publisher.
11. Ovsygannikova, I. A., Batsanova, S. S., Nasonova, L. I., Batsanova L. R., and Nakrasov, E. A., *Bull. Acad. Sc. USSR, Phys. Ser.* **31**, 936 (1967).
12. Hoppe, R., and Arend, K-H., *Z. Anorg. Allg. Chem.* **314**, 4 (1962).
13. Delgass, W. N., Boudart, M., and Parravano, G., *J. Phys. Chem.* **72**, 3563 (1968).